

# Scalable and Interpretable Marked Point Processes

Aristeidis Panos<sup>1,4</sup>, Ioannis Kosmidis<sup>1,4</sup>, and Petros Dellaportas<sup>2,3,4</sup>

<sup>1</sup>*Department of Statistics, University of Warwick, Coventry, UK*

<sup>2</sup>*Department of Statistical Science, University College London, London, UK*

<sup>3</sup>*Department of Statistics, Athens University of Economics and Business, Athens, Greece*

<sup>4</sup>*The Alan Turing Institute, London, UK*

## Abstract

We introduce a novel inferential framework for marked point processes that enjoys both scalability and interpretability. The framework is based on variational inference and it aims to speed up inference for a flexible family of marked point processes where the joint distribution of times and marks can be specified in terms of the conditional distribution of times given the process filtration, and of the conditional distribution of marks given the process filtration and the current time. We assess the predictive ability of our proposed method over four real-world datasets where results show its competitive performance against other baselines. The attractiveness of our framework for the modelling of marked point processes is illustrated through a case study of association football data where scalability and interpretability are exploited for extracting useful informative patterns.

## 1 Introduction

Point processes have been extensively used in a wide range of domains such as seismology [1, 2, 3], computational finance [4, 5], criminology [6], examining insurgence in Iraq [7], astronomy [8], neuroscience [9] to name a few. The recent advancement of information technologies, e.g. social media, electronic financial transactions, e-commerce systems etc, has provided an abundance of data where various types of events happen in irregular time intervals. The large amount of data and its complex dynamics paved the way of many deep learning applications [10, 11, 12, 13, 14, 15, 16] where an underlying neural net was able to capture non-linear relations between events. Despite of the ability of neural-based point processes to learn complex behavior from real-world data, their black-box nature limits them significantly in terms of intractability. A recent work [17] has developed a new family of marked point processes which provided both flexibility and interpretability through a decomposition of the joint distribution over times and marks. The resulting model has a directly interpretable parameterization and it has been use to model in-game event sequences from football data. Nevertheless, the inference process have been based on a Hamiltonian Monte Carlo algorithm [18], that quickly gets computationally prohibitive for large-scale event data sets.

In this work, we bridge the gap between lack of interpretability in neural-based point process models and the scalability issues of [17] by introducing an inferential framework based on variational inference (VI) that successfully deals with such limitations. Our contributions consist of (i) developing an implementation strategy that provides approximate posterior densities over model parameters instead of point estimates produced in state-of-the-art methods [11, 12, 16, 15], (ii) adopting a log-Normal model for the conditional distribution of times that outperforms other

state-of-the-art methods on predicting future events and marks, (iii) proposing computational and mathematical tricks that significantly reduce inference time without sacrificing performance and (iv) analysing a large dataset of touch-ball event data in football to demonstrate the scalability, interpretability, and extendibility of our proposed method. In particular, our model readily allows for feature-driven cross-excitation and learning of event genealogies, which allow the extraction of fruitful and insightful patterns about the game and the teams.

## 2 Background

### 2.1 Marked temporal point processes

A marked temporal point process (MTPP) [19] can be seen as an ordered sequence of event times  $t_i \in [0, T)$  over an observation interval  $[0, T)$ , accompanied by event marks  $u_i \in \mathcal{U}$ , which may include information about the event types or marks (discrete), location (continuous) or other event attributes. In this work we consider both discrete (multi-dimensional temporal point process) and continuous<sup>1</sup> (marked spatio-temporal point process) mark spaces  $\mathcal{U}$ . A MTPP is fully determined by its *conditional intensity function (CIF)*  $\lambda(t, u | \mathcal{F}_t)$  which gives the probability of observing an event in the space  $[0, T) \times \mathcal{U}$  given the filtration  $\mathcal{F}_t = \{(t_i, u_i) | t_i < t\}$ , i.e.  $\lambda(t, u | \mathcal{F}_t) ||B_{du}(u)|| dt = \mathbb{E}[N([t, t + dt] \times B_{du}(u)) | \mathcal{F}_t]$ , where  $N(A)$  is the counting measure of events over the set  $A \subseteq [0, T) \times \mathcal{U}$  and  $||B_{du}(u)||$  is the Lebesgue measure over the open ball of radius  $du > 0$  in  $\mathcal{U}$ . Given a dataset  $\mathcal{D} = \{\mathbf{y}_s\}_{s=1}^S$ , where  $\mathbf{y}_s = \{(t_i^{(s)}, u_i^{(s)})\}_{i=1}^{N_s}$  is the  $s$ -th sequence consisting of  $N_s$  time-mark pairs  $(t_i^{(s)}, u_i^{(s)})$ , the log-likelihood based on  $\mathcal{D}$  is

$$\ell^*(\mathcal{D}) = \sum_{s=1}^S \ell_s^*, \quad (1)$$

$$\text{where, } \ell_s^* = \sum_{i=1}^{N_s} \log \lambda(t_i^{(s)}, u_i^{(s)} | \mathcal{F}_{t_i^{(s)}}) - \int_0^T \int_{\mathcal{U}} \lambda(t, u | \mathcal{F}_{t^{(s)}}) du dt. \quad (2)$$

The  $*$  symbol in  $\ell^*$  indicates dependence on the filtration  $\mathcal{F}_t$ ,  $\mathcal{F}_{t^{(s)}} = \{(t_i^{(s)}, u_i^{(s)}) | t_i^{(s)} < t^{(s)}\}$  is the filtration of the  $s$ -th sequence, while dependence of  $\ell^*$  on other parameters is suppressed. Multivariate Hawkes process [1] is a well-studied MTPP, where past events contribute additively to the intensity of the current event, allowing in that way to capture mutual excitation (clustering) behaviour between events. The CIF of a multivariate Hawkes process with mark space  $\mathcal{U} = \{1, \dots, U\}$  is given by

$$\lambda(t, u | \mathcal{F}_t) = \mu \delta_u + \eta \sum_{j: t_j < t} \beta_{u_j, u} \exp(-\beta_{u_j, u}(t - t_j)) \gamma_{u_j, u}, \quad (3)$$

where  $\mu > 0$  is a constant background intensity,  $\delta_u > 0$  is the background probability for event type  $u$  with  $\sum_{u=1}^U \delta_u = 1$ ,  $\gamma_{u_j, u} > 0$  is the probability of triggering an event type  $u$  from the excitation of an event type  $u_j$  where  $\sum_{u=1}^U \gamma_{u_j, u} = 1$ ,  $\forall u_j \in \mathcal{U}$ , while  $\beta_{u_j, u} > 0$  is the exponential decay rate of that excitation. The parameter  $\eta \in (0, 1)$  is called the excitation factor.

### 2.2 Decoupled MTPP

Despite their widespread applicability in modelling event sequences [20, 6, 21], Hawkes processes perform poorly in cases where event times do not exhibit clustering behavior. This limitation

<sup>1</sup>We only considered the spatial component in our football case-study in Section 5.2, where we discretized the continuous space of the football field coordinates as in [17], and thus,  $\mathcal{U}$  was a discrete and finite space.

can be circumvented by considering the decomposition of the log-likelihood of a marked point process introduced in [17],

$$\ell_s^* = \sum_{i=1}^{N_s} \log f(u_i^{(s)} | t_i^{(s)}, \mathcal{F}_{t_i^{(s)}}; \boldsymbol{\theta}_f) + \sum_{i=1}^{N_s} \log g(t_i^{(s)} | \mathcal{F}_{t_i^{(s)}}; \boldsymbol{\theta}_g), \quad (4)$$

where  $f(\cdot)$  and  $g(\cdot)$  are the conditional probability mass function (PMF) of the event types and the conditional density for the occurrence times, respectively, parameterized by vectors  $\boldsymbol{\theta}_f$  and  $\boldsymbol{\theta}_g$ . The dependence of  $\ell_s^*$  on  $\boldsymbol{\theta}_f$  and  $\boldsymbol{\theta}_g$  has been suppressed to simplify notation. This decomposition allows to define a MTPP in terms of  $f(\cdot)$  and  $g(\cdot)$  instead of the CIF  $\lambda(t, u | \mathcal{F}_t)$ , providing extra flexibility to the specification of the model, and thus, added expressibility. For example, a gamma or a log-normal density could be chosen as  $g(\cdot)$  to capture non-clustering relations among time occurrences. In the current work, we adopt the same functional form of  $f(u_i^{(s)} | t_i^{(s)}, \mathcal{F}_{t_{i-1}^{(s)}}; \boldsymbol{\theta}_f)$  as in [17]

$$f(u_i^{(s)} | t_i^{(s)}, \mathcal{F}_{t_i^{(s)}}; \boldsymbol{\theta}_f) = \frac{\delta_{u_i^{(s)}} + \eta \sum_{j: t_j^{(s)} < t_i^{(s)}} \gamma_{u_j^{(s)}, u_i^{(s)}} \exp\left(-\beta_{u_j^{(s)}, u_i^{(s)}}(t_i^{(s)} - t_j^{(s)})\right)}{1 + \eta \sum_{j: t_j^{(s)} < t_i^{(s)}} \exp\left(-\beta_{u_j^{(s)}, u_i^{(s)}}(t_i^{(s)} - t_j^{(s)})\right)} \quad (5)$$

where  $\eta > 0$ , obtained by converting (3) into a PMF by normalising across all possible values of  $u$ . We denote the probability vector  $\boldsymbol{\delta} = (\delta_1, \dots, \delta_U)^\top$ , the stochastic matrix  $\Gamma \in [0, 1]^{U \times U}$  with  $\Gamma_{u, u'} = \gamma_{u, u'}$ , the decay matrix  $B \in \mathbb{R}_+^{U \times U}$  where  $B_{u, u'} = \beta_{u, u'}$ , so we have  $\boldsymbol{\theta}_f = \{\boldsymbol{\delta}, \Gamma, B, \eta\}$ .

The PMF of marks in (5) possesses a natural interpretation of its parameters. Large values of  $\eta$  correspond to higher dependence of each mark on its past events since  $\eta$  can be viewed as a scaling factor over the contributions of past events to the current event mark probability. The probabilities  $\gamma_{u_j, u}$  can be interpreted as the conversion rates for the transition from an event type  $u_j$  to an event type  $u$  while the decay rate  $\beta_{u, u'}$  quantifies the exponential rate at which the excitation from a previous event with mark  $u'$  decays over time given the current event with mark  $u$ . The background probability  $\delta_u$  gives the probability an event has a mark  $u$  given this event is triggered exclusively by a background (unknown) process. Having this interpretation, we can extract useful information regarding the cross-excitations between the event types and the corresponding decay rates over time for these excitations.

### 3 Proposed model

Despite the flexibility of the model introduced in [17], the suggested implementation is based on an MCMC algorithm that scales very poorly with number of time events, thus limiting its applicability only to small data sets. We address this limitation by introducing a variational Inference [22] (VI) implementation strategy which maintains the desirable properties of the model in [17], such as producing approximate posterior distributions over the parameters, while delivering vast computational speed-up over its MCMC counterpart. We focus on the PMF in (5), which, despite all the interpretability that brings into the model, is the computational bottleneck for the inference process.

**Variational inference.** By considering a variational distribution  $q_\xi(\boldsymbol{\theta}_f)$ , parameterized by the variational parameters  $\boldsymbol{\xi}$ , we aim to find these parameters that minimize the Kullback-Leibler divergence between the variational distribution  $q_\xi(\boldsymbol{\theta}_f)$  and the true posterior  $p_\xi(\boldsymbol{\theta}_f | \mathcal{D})$ . This is

equivalent to maximizing the *evidence lower bound* (ELBO) [22, 23] defined as

$$\text{ELBO}(\boldsymbol{\xi}, \boldsymbol{\nu}) := \mathbb{E}_{q_{\boldsymbol{\xi}}} \left[ \log \frac{p(\mathcal{D}|\boldsymbol{\theta}_f)p_{\boldsymbol{\nu}}(\boldsymbol{\theta}_f)}{q_{\boldsymbol{\xi}}(\boldsymbol{\theta}_f)} \right], \quad (6)$$

where  $p(\mathcal{D}|\boldsymbol{\theta}_f) := \prod_{s=1}^S \prod_{i=1}^{N_s} f(u_i^{(s)}|t_i^{(s)}, \mathcal{F}_{t_i}^{(s)}; \boldsymbol{\theta}_f)$  is the data likelihood, and  $p_{\boldsymbol{\nu}}(\boldsymbol{\theta}_f)$  is the prior depending on the hyperparameters  $\boldsymbol{\nu}$ , which are also chosen to maximize ELBO.

Regarding the variational distribution  $q_{\boldsymbol{\xi}}(\boldsymbol{\theta}_f)$ , we follow the mean-field approach where  $q_{\boldsymbol{\xi}}$  factorizes over  $\boldsymbol{\theta}_f$ , i.e.

$$q_{\boldsymbol{\xi}}(\boldsymbol{\theta}_f) = q_{\boldsymbol{\xi}}(\boldsymbol{\delta})q_{\boldsymbol{\xi}}(\Gamma)q_{\boldsymbol{\xi}}(B, \eta)$$

where each constituent distribution is defined as

$$q_{\boldsymbol{\xi}}(\boldsymbol{\delta}) = \text{Dir}(\boldsymbol{\alpha}_0), \quad (7)$$

$$q_{\boldsymbol{\xi}}(\Gamma) = \prod_{u=1}^U \text{Dir}(\boldsymbol{\alpha}_u), \quad (8)$$

$$q_{\boldsymbol{\xi}}(B, \eta) = \prod_{p=1}^{U^2+1} \text{Lognormal}(\mu_p, \sigma_p^2), \quad (9)$$

with  $\boldsymbol{\alpha}_p \in \mathbb{R}_+^U$ ,  $p = 0, 1, \dots, U$  being the concentration parameters of each Dirichlet distribution and  $\{\mu_p, \sigma_p^2\}_{p=1}^{U^2+1}$  are the means and variances of the log-normal distributions, and thus,  $\boldsymbol{\xi} = \{\{\boldsymbol{\alpha}_p\}_{p=0}^U, \{\mu_p, \sigma_p^2\}_{p=1}^{U^2+1}\}$ .

In order to maximize ELBO with respect to both  $\boldsymbol{\xi}, \boldsymbol{\nu}$ , we adopt a similar procedure as in [24] where a variational EM algorithm is employed to iteratively optimize (6). For calculating ELBO, we refer to black-box variational inference (BBVI) optimization [25, 26] where Monte Carlo integration is used to approximate the bound. The reparameterization trick in [26] allows us to obtain unbiased gradient estimates of the ELBO for the parameters of the log-normal distributions in (9). However, the reparameterization trick is not applicable to the concentration parameters  $\boldsymbol{\alpha}_i$ . To overcome this issue, we make use of pathwise gradients [27], allowing us to obtain an estimate of ELBO, given by

$$\text{ELBO}(\boldsymbol{\xi}, \boldsymbol{\nu}) \approx \frac{1}{L} \sum_{l=1}^L \log \frac{p(\mathcal{D}|\boldsymbol{\theta}_f^{(l)})p_{\boldsymbol{\nu}}(\boldsymbol{\theta}_f^{(l)})}{q_{\boldsymbol{\xi}}(\boldsymbol{\theta}_f^{(l)})}, \quad (10)$$

for  $L$  Monte Carlo samples  $\boldsymbol{\theta}_f^{(l)}$  generated from the variational distribution using the reparameterization trick/pathwise gradients. Following [24], we maximize (10) with respect to the variational parameters  $\boldsymbol{\xi}$  in the E-step while in the M-step we maximize with respect to the hyperparameters  $\boldsymbol{\nu}$ . The updated  $\boldsymbol{\nu}$  can be found in closed form when certain priors are utilized [24]. In this work we consider a zero-mean Gaussian prior over  $\eta$  and the entries of  $B$ , and thus, we need  $U^2 + 1$  hyperparameters to describe them. Furthermore, by imposing Dirichlet priors over  $\Gamma$  and  $\boldsymbol{\delta}$ , updating the concentration parameters of these priors is not required. This can be seen by expressing ELBO( $\lambda, \zeta$ ) as

$$\mathbb{E}_{q_{\boldsymbol{\xi}}} \left[ \log \frac{p(\mathcal{D}|\boldsymbol{\theta}_f)p_{\boldsymbol{\nu}}(\boldsymbol{\theta}_f)}{q_{\boldsymbol{\xi}}(\boldsymbol{\theta}_f)} \right] = \mathbb{E}_{q_{\boldsymbol{\xi}}} [\log p(\mathcal{D}|\boldsymbol{\theta}_f)] - \text{KL}[q_{\boldsymbol{\xi}}(\boldsymbol{\theta}_f) \parallel p_{\boldsymbol{\nu}}(\boldsymbol{\theta}_f)], \quad (11)$$

where  $\text{KL}[q||p]$  is the Kullback-Leibler (KL) divergence between distribution  $q$  and  $p$ . Notice that the above expression is maximized when the KL divergence is zero which is true for two Dirichlet

distributions when they share the same concentration parameters. Hence, these Dirichlet priors can be safely ignored from the ELBO and no hyperparameter update is required at the M-step. More details regarding the derivation of ELBO and the optimization procedure can be found in Section A of Appendix.

**Computational speed-up.** The above model, despite its flexibility, still suffers from scalability issues due to the log-likelihood term  $\log p(\mathcal{D}|\boldsymbol{\theta}_f)$  which scales as  $\mathcal{O}(SN^2)$  where  $N = \max_{s=1, \dots, S} |\mathbf{y}_s|$ . To circumvent the problem, we assume that past events do not contribute to the evaluation of the summation term in (5) up to a point, and thus, they can be ignored from the computation. This reduces time complexity to  $\mathcal{O}(SQN)$ , where  $Q \ll N$  is the number of past events we choose to be considered at the evaluation of (5), constituting inference feasible for large-scale datasets. This assumption can be justified by the fact that large time intervals  $t_i - t_j$  lead to near to zero contributions for past events  $t_j$ , and hence, their absence would not affect the final log-likelihood value.  $Q$  is a tunable hyperparameter which can be determined by inspecting the values of the log-likelihood on a validation dataset. Similar cut-off assumptions to speed-up computations have been also considered in [28, 29]. The overall complexity is affected by the number of Monte Carlo samples  $M$ . However,  $M = 1$  is usually sufficient for BBVI applications as previous studies indicate [26, 24]. Finally, to further alleviate the computational burden, we approximate (1) by randomly selecting batches of sequences  $\mathcal{B} \subseteq \{1, 2, \dots, S\}$ , and taking unbiased estimates as follows,

$$\sum_{s=1}^S \ell_s^* \approx \frac{S}{|\mathcal{B}|} \sum_{s' \in \mathcal{B}} \ell_{s'}^*.$$

**Time modelling.** Time occurrences are modelled by log-normal distributions as follows,

$$g(t_i|\mathcal{F}_{t_i}; \boldsymbol{\theta}_g) = p(r_i|u_{i-1}, \tilde{\boldsymbol{\mu}}, \tilde{\boldsymbol{\sigma}}), \quad (12)$$

where  $r_i := t_i - t_{i-1}$ ,  $t_0 = 0$ ,  $\tilde{\boldsymbol{\mu}} \in \mathbb{R}^U$ ,  $\tilde{\boldsymbol{\sigma}} \in \mathbb{R}_+^U$  are the means and standard deviations of the log-normal distributions, respectively, with density  $p(r_i)$ . Therefore, the inter-arrival times  $r_i$  are log-normally distributed where the distribution's parameters depend on the value of the previous mark  $u_{i-1}$ , i.e.

$$r_i \sim \text{Lognormal}(\tilde{\boldsymbol{\mu}}_{u_{i-1}}, \tilde{\boldsymbol{\sigma}}_{u_{i-1}}^2). \quad (13)$$

In a similar way, we could consider any continuous distribution with support on the positive reals for the inter-arrival times, such as gamma. However, we found that log-normal distributions are sufficient for the real-world datasets considered in Section 5. Note also that the distribution over inter-arrival times allows for the easy and fast prediction of future time events. This is in contrast to prediction for CIF-based models, which requires computationally demanding procedures, like Ogata's modified thinning algorithm [20]. Specifically, for a point process with CIF  $\lambda(t)$ , a prediction of the next time occurrence  $t^*$  is computed as

$$t^* = \mathbb{E}[\tilde{t}|\mathcal{F}_t] = \int_t^\infty \tilde{t} \lambda(\tilde{t}|\mathcal{F}_t) \exp\left(-\int_t^{\tilde{t}} \lambda(u|\mathcal{F}_t) du\right) d\tilde{t}, \quad (14)$$

which is intractable, and Monte Carlo sampling via Ogata's algorithm is used to estimate it. In our formulation, we simply use the mode of the log-normal distribution to predict the next time occurrence.

**Interpretability** The interpretation of the model’s parameters is one of the main advantages of choosing (5) as the probability mass function of marks. Parameters’ interpretability is quite common for simple parametric point process models such as the multivariate Hawkes process [1, 30, 31], nevertheless, state-of-the-art methods scalable based on neural nets (NNs) [32, 11, 13, 15] lack this interpretation, and thus, they are viewed as black boxes. Recently, a new method based on a combination of NN and the attentive mechanism [16], has outperformed the rest of the NN-based baselines in terms of predictive power while presenting more interpretability than its competitors. However, this interpretability comes from a latent vector which is learned throughout training and it has no natural interpretation as the parameters of the proposed model.

## 4 Related work

There is a voluminous literature on modelling event sequences with a vast proportion of it focused on Hawkes process models [1] and their variants [33, 31, 34, 35, 36, 37, 38, 39, 40, 41, 29, 42]. Most of these methods are concerned with parametric forms of the intensity functions which generalize Hawkes processes and they aim to learn non-parametrically the so-called triggering kernels which model the dependencies between events. The non-parametric nature of these methods adds extra flexibility at the expense of interpretability. For instance, [31] introduce a method that learns triggering kernels by solving ordinary differential equations via discretization while [40], in the same spirit, attains this learning by solving a least-square problem. There are also works where the whole conditional intensity function is learned non-parametrically based on Gaussian processes [43], allowing to capture the complex events’ dynamics [28, 44, 45]. Nevertheless, interpretability is further reduced in tandem with scalability due to the computationally demanding linear algebra required for training these models. A more scalable solution that maintains flexibility is based on the introduction of deep learning techniques [10, 11, 46, 12, 16, 15] that has produced state-of-the-art results in the field. The majority of these methods develop variants of recurrent neural networks (RNN) which aim to model the intensity function of a point process. Recently, [15] has proposed a method which, instead of modelling the CIF, it models the conditional distribution of the inter-arrival times using a log-normal mixture density network. Interpretability in these methods is once again limited due to the black-box nature of the neural networks. Finally, our work bears similarities mainly with the VI framework of learning Hawkes process in [24] and the MCMC-based method of decoupled marked point processes in [17], however, the former suffers from flexibility limitations while the latter faces severe scalability issues.

## 5 Experiments

In Section 5.1 we investigate the predictive performance of the proposed model, which we term *VI-Decomposable Point process (VI-DPP)*, over four real-world datasets and compare the results to state-of-the-art baselines. Furthermore, in Section 5.2, a thorough examination of the interpretability of the model is carried out over a case study that involves football data. Our code, based on PyTorch [47], is publicly available at <https://github.com/aresPanos/Interpretable-Point-Processes>.

## 5.1 Real-world datasets

We consider four real-world datasets spanning over different properties such as number of sequences  $S$ , total number of events, mean sequence length etc; see Table 1. A detailed description of each of the datasets can be found in Appendix C. Our method is trained on these four datasets and results are compared to those of three other baselines. We pick for comparisons the VI-based Hawkes process variant in [24] due to its state-of-the-art performance over other MLE-based methods. We use both a parametric version with an exponential triggering function (*VI-EXP*) and a non-parametric one with mixture of Gaussians triggering function (*VI-SG*). This method resembles ours in the way that inference is performed, however, it is limited to a parameterized form of a Hawkes process CIF and it requires careful hyperparameter tuning which is usually computationally demanding for large-scale applications. We also include in our comparisons the state-of-the-art NN-based method *Self-Attentive Hawkes Process (SAHP)* [16] which utilizes the self-attention mechanism [48] to address the effect of long-range/non-linear dependencies.

We randomly split each dataset in ten train/validation/test (70%/10%/20%) sets. The train data set is used for inference, the validation dataset is used for tuning the hyperparameters, and the predictive performance is evaluated on test dataset. Predictive performance is assessed by three different metrics: (i) mean log-likelihood (LLKL) for the ability of each method to model event sequences, (ii) root-mean-square error (RMSE) for the ability of each method to predict future time events, and (iii)  $F_1$  score for the ability of each method to predict future marks. RMSE is computed as in [16], as the square-root of the sum of the squares of  $\epsilon_i = (t_{i+1}^* - t_i)/(t_{i+1} - t_i) - 1$ , where  $t_{i+1}^*$  is the predicted time of the next event.  $F_1$  score is chosen to take into account possible mark imbalances. Regarding mark prediction, since our VI method gives a distribution over the parameters  $\theta_f$  and not a point estimate, the PMF in (5) is computed using the mode of the log-normal distribution in (9) and the mean of the Dirichlet distributions in (7), (8). Further experimental details are given in Appendix B. The results are reported in Table 2.

We see that VI-DPP consistently outperforms the other baselines in terms of both RMSE and  $F_1$ , providing evidence for the flexibility of the decoupled MTPP. SAHP scores higher values of LLKL due to the flexibility of the NN which is based on. We also notice a significant speed-up of our method over the rest competitors for all datasets but the Retweets. This is because a small number of cut-off points  $Q$  is enough to achieve good results for the first three datasets while for Retweet we had to use a larger number; see Appendix B. It is worth mentioning that our method required minimal hyperparameter tuning in contrast to the other three baselines where meticulous hyperparameter tuning was crucial for achieving competitive results. This process leads to considerably higher computational times, especially for large-scale datasets, something that is not directly revealed in Table 2. Moreover, it is investigated how  $Q$  affects the performance of our model in terms of RMSE,  $F_1$  score, and training time over the Retweets dataset; see Figure 3 of Appendix. Values of  $Q > 20$  do not provide any significant performance boost for both RMSE and  $F_1$  while training time, as theory implies, increases linearly with respect to  $Q$ .

## 5.2 Case study: Association Football

The data used in this study consist of all touch-ball events recorded in all English Premier League (EPL) games throughout the season 2013/2014. Each sequence includes the touch events from one of the two halves of each game. Hence, we have 720 sequences for 380 games between 20 teams for the season and more than half a million touch-ball events. The dataset consists of triplets  $(t, u, z)$ , where  $t$  is the time when the touch-ball event occurred,  $u$  is the event type with

Table 1: Characteristics of real-world datasets.  $U$ ,  $S$ ,  $\#$ , are the numbers of marks, sequences, and events (in thousands), respectively. TR, VA, and TE are training, validation, and test, respectively

DATASET	$U$	SEQUENCE LENGTHS			$S$			$\#$		
		MIN	MAX	MEAN	TR	VA	TE	TR	VA	TE
MIMIC [49, 10]	75	2	33	4	454	66	130	1.6	0.25	0.5
SOF [10]	22	41	736	72	4643	663	1327	336	47	95
MOOC [50]	97	4	493	56	4932	705	1410	279	37	79
RET [51]	3	50	264	109	16800	2400	4800	1825	262	522

Table 2: Performance comparison between our proposed model (VI-DPP) and three other baselines over the four real-world datasets of Section 5.1. Bold results indicate superior performance across the four competing approaches.

METHODS	METRICS	MIMIC		SOF		MOOC		RET	
VI-EXP	LLKL	-3.072	(0.148)	-2.523	(0.022)	-1.387	(0.024)	-0.733	(0.005)
	RMSE	3.075	(0.897)	71.175	(9.970)	112.805	(6.951)	332.604	(83.590)
	$F_1$	<b>82.28</b>	(5.54)	5.52	(0.60)	10.10	(0.38)	41.21	(0.52)
	TIME (MIN)	116.53	(15.29)	99.92	(21.78)	842.44	(133.20)	67.19	(10.85)
VI-GAUSS	LLKL	-3.070	(0.144)	-2.461	(0.022)	-4.260	(0.041)	0.238	(0.011)
	RMSE	5.190	(1.817)	53.778	(10.098)	5436.984	(486.614)	319.599	(37.234)
	$F_1$	80.77	(4.59)	5.64	(0.86)	5.57	(0.41)	40.78	(0.82)
	TIME (MIN)	248.94	(118.58)	586.13	(49.86)	1400.96	(128.93)	<b>61.57</b>	(17.65)
SAHP	LLKL	<b>1.534</b>	(0.215)	<b>-0.506</b>	(0.006)	<b>1.289</b>	(0.136)	0.621	(1.670)
	RMSE	10.896	(2.447)	44.968	(4.450)	28.409	(12.342)	354.880	(26.162)
	$F_1$	63.60	(6.38)	8.45	(0.31)	14.07	(0.95)	41.31	(0.70)
	TIME (MIN)	63.09	(1.64)	398.21	(21.17)	528.34	(26.81)	80.54	(24.70)
VI-DPP	LLKL	-1.680	(0.074)	-2.394	(0.032)	-0.246	(0.056)	<b>1.162</b>	(0.020)
	RMSE	<b>2.174</b>	(1.380)	<b>5.385</b>	(1.190)	<b>0.994</b>	(0.000)	<b>1.000</b>	(0.001)
	$F_1$	60.03	(6.79)	<b>10.27</b>	(0.26)	<b>19.34</b>	(0.50)	<b>41.35</b>	(0.04)
	TIME (MIN)	<b>3.71</b>	(0.46)	<b>82.19</b>	(5.93)	<b>121.54</b>	(14.20)	677.30	(0.01)

$u \in \{1, \dots, 30\}$  and  $z \in \{1, 2, 3\}$  denotes the spatial location, or zone, in the football field that the event took place. In reality there are 15 distinct types but they are labelled by which team (home or away) triggered this event; see Table 3 in Appendix and [17] for a detailed description of the data, including statistics and pre-processing steps.

Our analysis here uses an extension of (5) that accounts for the zone-information as

$$f(u_i^{(s)} | t_i^{(s)}, z_i^{(s)}, \mathcal{F}_{t_i^{(s)}}) = \frac{\delta_{u_i^{(s)}}^{z_i^{(s)}} + \alpha \sum_{j: t_j^{(s)} < t_i^{(s)}} \gamma_{u_j^{(s)}, u_i^{(s)}}^{z_i^{(s)}} \exp\left(-\beta_{u_j^{(s)}, u_i^{(s)}}^{z_i^{(s)}}(t_i^{(s)} - t_j^{(s)})\right)}{1 + \alpha \sum_{j: t_j^{(s)} < t_i^{(s)}} \exp\left(-\beta_{u_j^{(s)}, u_i^{(s)}}^{z_i^{(s)}}(t_i^{(s)} - t_j^{(s)})\right)}. \quad (15)$$

The parameters  $\delta, \Gamma, B$  are now location specific, i.e.  $\delta_u^z = \delta_{u,u'}^z, \Gamma_{u,u'}^z = \gamma_{u,u'}^z$ , and  $B_{u,u'}^z = \beta_{u,u'}^z$ . We also incorporate team information via the following baseline-category logit representation of  $\Gamma$

$$\log\left(\frac{\gamma_{u,u'}^z(c)}{\gamma_{u,u}^z(c)}\right) = \phi_{u,u'}^z + \omega_{cu'}, \quad u' = 1, \dots, U-1, \quad c = 1, \dots, 20, \quad (16)$$



where  $\phi_{u,u'}^z$  is a location-specific base parameter and  $\omega_{cu'}$  represents the ability of the team in position  $c$  to complete a conversion to an event of type  $u'$ . The new model defined by (15) and (16) can be easily incorporated in the VI framework of Section 3. We set a univariate normal distribution for  $\phi_{u,u'}^z$  and  $\omega_{cu'}$  and we learn each parameters by maximizing the ELBO. The total number of variational parameters is 12092.

We trained our model on bi-weekly data that includes events from two consecutive matchweeks, i.e. 20 games (or 40 sequences). Each dataset of 20 games consists of 27,587 ( $\pm 296$ ) events on average. This process is repeated for all 380 matches leading to 19 different sets of optimized parameters. In all cases our model was trained for 2000 epochs without minibatches and  $Q = 5$ .

In Figure 1, we investigate how the ability of passing unsuccessfully and the scoring ability for each team evolves through the season. We clearly see that teams ranked in the top positions of the league table are less able to pass unsuccessfully, while their corresponding scoring ability is consistently high. On the other hand, bottom-ranked teams exhibit the exact opposite behaviour, confirming the intuition that teams who can score and pass accurately finish at higher places of the league table. Similar heatmaps for the rest of the abilities are given in Appendix.

Next, we formulate a team-specific ordinal regression model to examine which of the fifteen distinct abilities is more important for predicting the number of points won by each team in two consecutive matches. We use as features the estimated unsuccessful passing and scoring abilities for each team. Each dataset consists of 19 data points in total. Unsurprisingly, the regression coefficient with the largest value is the Goal ability since this is the most crucial factor for a team to earn points.

Finally, we use our model to recover event genealogies using its hidden *branching structure* [2]. The branching structure of categorizes the events into *immigrants* and *offsprings*. Offspring events are triggered by previous events while immigrant events are not linked with a parent event. Let  $w_i^{(s)}$  be the random variable indicating whether the  $i$ -th event of the  $s$ -th sequence is an immigrant ( $w_i^{(s)} = 0$ ) or an offspring ( $w_i^{(s)} = j$ ) of a previous event indexed by  $j$ , we can calculate analytically the conditional branching structure probabilities as

$$p(w_i^{(s)} = 0 | \mathcal{F}_{t_i^{(s)}}) = \frac{\delta_{u_i^{(s)}}^{z_i^{(s)}}}{\delta_{u_i^{(s)}}^{z_i^{(s)}} + \alpha \sum_{k: t_k^{(s)} < t_i^{(s)}} \gamma_{u_k^{(s)}, u_i^{(s)}}^{z_i^{(s)}} \exp\left(-\beta_{u_k^{(s)}, u_i^{(s)}}^{z_i^{(s)}}(t_i^{(s)} - t_k^{(s)})\right)},$$

$$p(w_i^{(s)} = j | \mathcal{F}_{t_i^{(s)}}) = \begin{cases} \frac{\gamma_{u_j^{(s)}, u_i^{(s)}}^{z_i^{(s)}} \exp\left(-\beta_{u_j^{(s)}, u_i^{(s)}}^{z_i^{(s)}}(t_i^{(s)} - t_j^{(s)})\right)}{\delta_{u_i^{(s)}}^{z_i^{(s)}} + \alpha \sum_{k: t_k^{(s)} < t_i^{(s)}} \gamma_{u_k^{(s)}, u_i^{(s)}}^{z_i^{(s)}} \exp\left(-\beta_{u_k^{(s)}, u_i^{(s)}}^{z_i^{(s)}}(t_i^{(s)} - t_k^{(s)})\right)}, & \text{if } t_j^{(s)} < t_i^{(s)} \\ 0, & \text{otherwise.} \end{cases}$$

The above probabilities are based on the model in (15) and their computation allows us to gain insights over the causality of the event occurrences by assuming a causal constraint that any event is triggered by exactly one of the previous events or the background. Hence, this calculation of probabilities attains the recovering of the hidden branching structure  $w_i^{(s)}$ . We choose four different matches of the 2013/14 EPL winner Manchester City (MC) and we build the branching structure taking into account the last ten events before a MC's player scores the first goal in the first half of the game. More details are given in caption of Figure 2. To gain better intuition of how this experiment is related to the real matches we provide the links of the videos with the goals scored from these four matches in Appendix. For panel (a) of Figure 2 we observe that our model suggests the event "H\_Dribble", the third event before the first

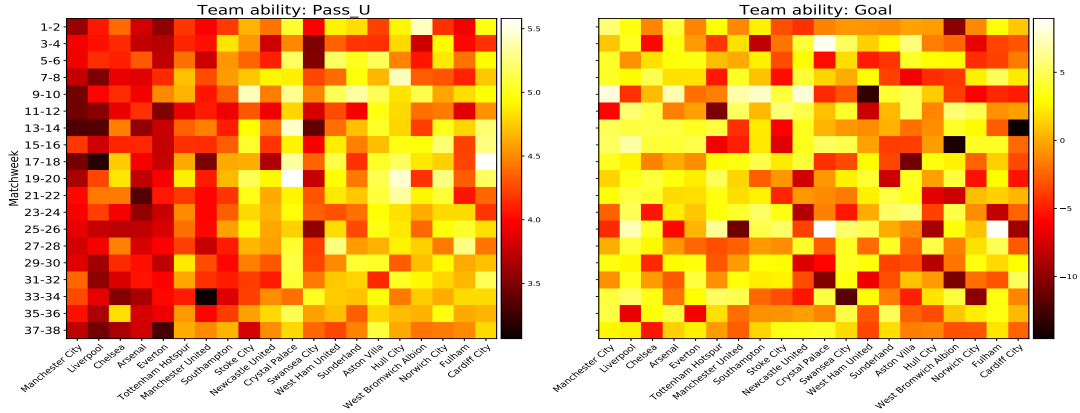


Figure 1: Heatmaps illustrating the evolution of unsuccessful passing (left panel) and scoring (right panel) ability for each team across the season. The ability is computed by adding the home and away abilities for each team using the optimized values of  $\{\omega_{cu}\}_{c,u}$  from each of the 19 bi-weekly datasets. The teams on the x-axis are shown in decreasing order of final ranking in the 2013/2014 EPL while the y-axis gives the corresponding matchweeks used for training our model.

goal is scored, is the most probable event that leads to this goal. Interestingly, by watching the corresponding video, we observe that this event plays a crucial role for scoring this goal since MC’s player Silva by dribbling/conveying the ball closer to opponent’s goal area creates the right circumstances for scoring the goal himself. Panel (b) shows that the last two successful passes of MC are the events that most probably lead to scoring which can be verified by the corresponding video. Panel (c) indicates that surely the goal is scored after a free-kick of MC which indeed was the case. Finally, in panel (d), the branching structure suggests that the goal was not a result of past known events, but instead it was an immigrant event. The video of the goal interestingly verifies that this goal was luckily scored by MC’s player Silva after the ball bounced against the opponent goalkeeper and the right goalpost before it landed to Silva’s feet. It is encouraging that our model is able to capture such level of detail in football dynamics while preserving interpretability.

## 6 Conclusion

We have proposed a novel extensible inferential framework for a flexible family of interpretable MTPPs based on VI and associated computational tricks that allows scalable training for large-scale time-event data, while maintaining a natural interpretation of the model parameters. Experiments on real-world datasets have demonstrated the competitiveness of our method over state-of-the art alternatives including some involving neural network specifications. We have carried out a case study based on a large volume of football events data where the scalability and interpretability of our method has lead to valuable insights of in-match dynamics.

The majority of existing methods in Section 4 do not account for spatial information because of the extra computational effort and complexity. In contrast, the VI-DPP methodology applies

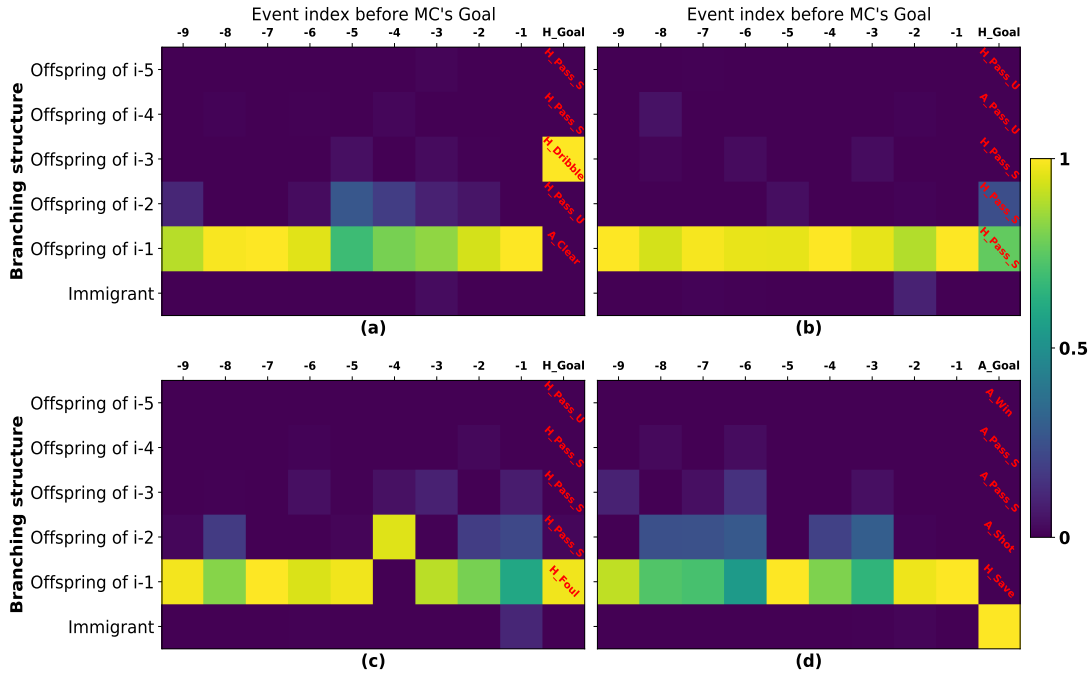


Figure 2: Branching structure of the last 10 events before the first goal scored by Manchester City in the first half of the game from four different matches played by Manchester City (MC). The games are (a) MC vs Newcastle United on 19/08/2013, (b) MC vs Manchester United on 01/12/2013, (c) MC vs Swansea City, and (d) Arsenal vs MC on 29/03/2014. Each plot reads bottom-up with each column representing a probability vector which gives the probability the event on x-axis is triggered by an immigrant or by an offspring occurred at most 5 events in advance. The last column always depicts the sequence of the last 5 events (event types in red) before the MC scores. The prefixes 'H' or 'A' indicate whether MC is the home or away team and the suffixes 'U' and 'S' indicate whether the passes were unsuccessful or successful, respectively.

directly on extensions of model (4) like

$$\ell_s^* = \sum_{i=1}^{N_s} \log f(u_i^{(s)} | t_i^{(s)}, z_i^{(s)}, \mathcal{F}_{t_i^{(s)}}; \boldsymbol{\theta}_f) + \sum_{i=1}^{N_s} \log h(z_i^{(s)} | t_i^{(s)}, \mathcal{F}_{t_i^{(s)}}; \boldsymbol{\theta}_h) + \sum_{i=1}^{N_s} \log g(t_i^{(s)} | \mathcal{F}_{t_i^{(s)}}; \boldsymbol{\theta}_g),$$

where  $h(\cdot | t_i^{(s)}, \mathcal{F}_{t_i^{(s)}})$  is the conditional PMF for discrete space; Section 5.2 illustrates this fact. The extensions for continuous spatial information require more involved parameterizations of  $f(\cdot | t_i^{(s)}, z_i^{(s)}, \mathcal{F}_{t_i^{(s)}})$  and they are the subject of further work. Another promising direction for future research that we currently investigate is the adaptation of VI-DPP for the online learning of MTPPs using stochastic gradient descent for real-time applications.

## References

- [1] Alan G Hawkes. Spectra of some self-exciting and mutually exciting point processes. *Biometrika*, 58(1):83–90, 1971.
- [2] Alan G Hawkes and David Oakes. A cluster process representation of a self-exciting process. *Journal of Applied Probability*, pages 493–503, 1974.
- [3] Yosihiko Ogata. Space-time point-process models for earthquake occurrences. *Annals of the Institute of Statistical Mathematics*, 50(2):379–402, 1998.
- [4] Emmanuel Bacry, Adrian Iuga, Matthieu Lasnier, and Charles-Albert Lehalle. Market impacts and the life cycle of investors orders. *Market Microstructure and Liquidity*, 1(02):1550009, 2015.
- [5] Emmanuel Bacry, Thibault Jaisson, and Jean-François Muzy. Estimation of slowly decreasing hawkes kernels: application to high-frequency order book dynamics. *Quantitative Finance*, 16(8):1179–1201, 2016.
- [6] George O Mohler, Martin B Short, P Jeffrey Brantingham, Frederic Paik Schoenberg, and George E Tita. Self-exciting point process modeling of crime. *Journal of the American Statistical Association*, 106(493):100–108, 2011.
- [7] Erik Lewis, George Mohler, P Jeffrey Brantingham, and Andrea L Bertozzi. Self-exciting point process models of civilian deaths in iraq. *Security Journal*, 25(3):244–264, 2012.
- [8] PC Gregory and Thomas J Lored. A new method for the detection of a periodic signal of unknown shape and period. *The Astrophysical Journal*, 398:146–168, 1992.
- [9] John P Cunningham, Byron M Yu, Krishna V Shenoy, and Maneesh Sahani. Inferring neural firing rates from spike trains using gaussian processes. *Advances in neural information processing systems*, 20:329–336, 2007.
- [10] Nan Du, Hanjun Dai, Rakshit Trivedi, Utkarsh Upadhyay, Manuel Gomez-Rodriguez, and Le Song. Recurrent marked temporal point processes: Embedding event history to vector. In *Proceedings of the 22nd ACM SIGKDD International Conference on Knowledge Discovery and Data Mining*, pages 1555–1564, 2016.
- [11] Hongyuan Mei and Jason M Eisner. The neural Hawkes process: A neurally self-modulating multivariate point process. In *Advances in Neural Information Processing Systems*, pages 6754–6764, 2017.

- [12] Shuang Li, Shuai Xiao, Shixiang Zhu, Nan Du, Yao Xie, and Le Song. Learning temporal point processes via reinforcement learning. In *Proceedings of the 32nd International Conference on Neural Information Processing Systems*, pages 10804–10814, 2018.
- [13] Takahiro Omi, Naonori Ueda, and Kazuyuki Aihara. Fully neural network based model for general temporal point processes. *arXiv preprint arXiv:1905.09690*, 2019.
- [14] Hengguan Huang, Hao Wang, and Brian Mak. Recurrent poisson process unit for speech recognition. In *Proceedings of the AAAI Conference on Artificial Intelligence*, volume 33, pages 6538–6545, 2019.
- [15] Oleksandr Shchur, Marin Biloš, and Stephan Günnemann. Intensity-free learning of temporal point processes. In *International Conference on Learning Representations*, 2019.
- [16] Qiang Zhang, Aldo Lipani, Omer Kirnap, and Emine Yilmaz. Self-attentive Hawkes process. In *International Conference on Machine Learning*, pages 11183–11193. PMLR, 2020.
- [17] Santhosh Narayanan, Ioannis Kosmidis, and Petros Dellaportas. Flexible marked spatio-temporal point processes with applications to event sequences from association football. *arXiv preprint arXiv:2103.04647*, 2021.
- [18] Simon Duane, Anthony D Kennedy, Brian J Pendleton, and Duncan Roweth. Hybrid monte carlo. *Physics letters B*, 195(2):216–222, 1987.
- [19] Alex Reinhart et al. A review of self-exciting spatio-temporal point processes and their applications. *Statistical Science*, 33(3):299–318, 2018.
- [20] Yosihiko Ogata. On Lewis’ simulation method for point processes. *IEEE transactions on information theory*, 27(1):23–31, 1981.
- [21] Clive G Bowsher. Modelling security market events in continuous time: Intensity based, multivariate point process models. *Journal of Econometrics*, 141(2):876–912, 2007.
- [22] David M Blei, Alp Kucukelbir, and Jon D McAuliffe. Variational inference: A review for statisticians. *Journal of the American statistical Association*, 112(518):859–877, 2017.
- [23] Cheng Zhang, Judith Bütepage, Hedvig Kjellström, and Stephan Mandt. Advances in variational inference. *IEEE transactions on pattern analysis and machine intelligence*, 41(8):2008–2026, 2018.
- [24] Farnood Salehi, William Trouleau, Matthias Grossglauser, and Patrick Thiran. Learning Hawkes processes from a handful of events. In *Advances in Neural Information Processing Systems*, pages 12715–12725, 2019.
- [25] Rajesh Ranganath, Sean Gerrish, and David Blei. Black box variational inference. In *Artificial intelligence and statistics*, pages 814–822. PMLR, 2014.
- [26] Diederik P Kingma and Max Welling. Auto-encoding variational bayes. *arXiv preprint arXiv:1312.6114*, 2013.
- [27] Martin Jankowiak and Fritz Obermeyer. Pathwise derivatives beyond the reparameterization trick. In *International Conference on Machine Learning*, pages 2235–2244, 2018.
- [28] Siqi Liu and Milos Hauskrecht. Nonparametric regressive point processes based on conditional Gaussian processes. In *Advances in Neural Information Processing Systems*, pages 1064–1074, 2019.

- [29] Rui Zhang, Christian Walder, and Marian-Andrei RizoIU. Variational inference for sparse gaussian process modulated Hawkes process. In *Proceedings of the AAAI Conference on Artificial Intelligence*, volume 34, pages 6803–6810, 2020.
- [30] Manuel Gomez-Rodriguez, Jure Leskovec, and Andreas Krause. Inferring networks of diffusion and influence. *ACM Transactions on Knowledge Discovery from Data (TKDD)*, 5(4):1–37, 2012.
- [31] Ke Zhou, Hongyuan Zha, and Le Song. Learning triggering kernels for multi-dimensional Hawkes processes. In *International Conference on Machine Learning*, pages 1301–1309, 2013.
- [32] Nan Du, Mehrdad Farajtabar, Amr Ahmed, Alexander J Smola, and Le Song. Dirichlet-Hawkes processes with applications to clustering continuous-time document streams. In *Proceedings of the 21th ACM SIGKDD International Conference on Knowledge Discovery and Data Mining*, pages 219–228, 2015.
- [33] David Marsan and Olivier Lengline. Extending earthquakes’ reach through cascading. *Science*, 319(5866):1076–1079, 2008.
- [34] Remi Lemonnier and Nicolas Vayatis. Nonparametric markovian learning of triggering kernels for mutually exciting and mutually inhibiting multivariate Hawkes processes. In *Joint European Conference on Machine Learning and Knowledge Discovery in Databases*, pages 161–176. Springer, 2014.
- [35] Niels Richard Hansen, Patricia Reynaud-Bouret, Vincent Rivoirard, et al. Lasso and probabilistic inequalities for multivariate point processes. *Bernoulli*, 21(1):83–143, 2015.
- [36] Hongteng Xu, Mehrdad Farajtabar, and Hongyuan Zha. Learning Granger causality for Hawkes processes. In *International conference on machine learning*, pages 1717–1726, 2016.
- [37] Emmanuel Bacry and Jean-Francois Muzy. First- and second-order statistics characterization of Hawkes processes and non-parametric estimation. *IEEE Transactions on Information Theory*, 62(4):2184–2202, 2016.
- [38] Yichen Wang, Bo Xie, Nan Du, and Le Song. Isotonic Hawkes processes. In *International conference on machine learning*, pages 2226–2234. PMLR, 2016.
- [39] Young Lee, Kar Wai Lim, and Cheng Soon Ong. Hawkes processes with stochastic excitations. In *International Conference on Machine Learning*, pages 79–88. PMLR, 2016.
- [40] Michael Eichler, Rainer Dahlhaus, and Johannes Dueck. Graphical modeling for multivariate Hawkes processes with nonparametric link functions. *Journal of Time Series Analysis*, 38(2):225–242, 2017.
- [41] Baichuan Yuan, Hao Li, Andrea L Bertozzi, P Jeffrey Brantingham, and Mason A Porter. Multivariate spatiotemporal Hawkes processes and network reconstruction. *SIAM Journal on Mathematics of Data Science*, 1(2):356–382, 2019.
- [42] Sophie Donnet, Vincent Rivoirard, Judith Rousseau, et al. Nonparametric bayesian estimation for multivariate Hawkes processes. *Annals of Statistics*, 48(5):2698–2727, 2020.
- [43] Carl Edward Rasmussen and Christopher K. I. Williams. *Gaussian processes for machine learning*, volume 2. MIT press Cambridge, MA, 2006.

- [44] Chris Lloyd, Tom Gunter, Michael Osborne, Stephen Roberts, and Tom Nickson. Latent point process allocation. In *Artificial Intelligence and Statistics*, pages 389–397, 2016.
- [45] Hongyi Ding, Mohammad Khan, Issei Sato, and Masashi Sugiyama. Bayesian nonparametric Poisson-process allocation for time-sequence modeling. In *International Conference on Artificial Intelligence and Statistics*, pages 1108–1116, 2018.
- [46] Shuai Xiao, Mehrdad Farajtabar, Xiaojing Ye, Junchi Yan, Xiaokang Yang, Le Song, and Hongyuan Zha. Wasserstein learning of deep generative point process models. In *Advances in Neural Information Processing Systems 30*, 2017.
- [47] Adam Paszke, Sam Gross, Francisco Massa, Adam Lerer, James Bradbury, Gregory Chanan, Trevor Killeen, Zeming Lin, Natalia Gimelshein, Luca Antiga, et al. Pytorch: An imperative style, high-performance deep learning library. *Advances in Neural Information Processing Systems*, 32:8026–8037, 2019.
- [48] Ashish Vaswani, Noam Shazeer, Niki Parmar, Jakob Uszkoreit, Llion Jones, Aidan N Gomez, Lukasz Kaiser, and Illia Polosukhin. Attention is all you need. In *NIPS*, 2017.
- [49] Alistair EW Johnson, Tom J Pollard, Lu Shen, H Lehman Li-Wei, Mengling Feng, Mohammad Ghassemi, Benjamin Moody, Peter Szolovits, Leo Anthony Celi, and Roger G Mark. Mimic-iii, a freely accessible critical care database. *Scientific data*, 3(1):1–9, 2016.
- [50] Srijan Kumar, Xikun Zhang, and Jure Leskovec. Predicting dynamic embedding trajectory in temporal interaction networks. In *Proceedings of the 25th ACM SIGKDD International Conference on Knowledge Discovery & Data Mining*, pages 1269–1278, 2019.
- [51] Qingyuan Zhao, Murat A Erdogdu, Hera Y He, Anand Rajaraman, and Jure Leskovec. Seismic: A self-exciting point process model for predicting tweet popularity. In *Proceedings of the 21th ACM SIGKDD international conference on knowledge discovery and data mining*, pages 1513–1522, 2015.
- [52] Diederik P Kingma and Jimmy Ba. Adam: A method for stochastic optimization. *arXiv preprint arXiv:1412.6980*, 2014.

# Appendix

## A On the derivation of VI-DPP

The ELBO defined in (6) can be also seen as a lower bound on the log-marginal likelihood

$$\log p(\mathcal{D}; \boldsymbol{\nu}) := \log \int p(\mathcal{D}|\boldsymbol{\theta}_f) p_{\boldsymbol{\nu}}(\boldsymbol{\theta}_f) d\boldsymbol{\theta}_f,$$

where a direct application of Jensen’s inequality gives

$$\log p(\mathcal{D}; \boldsymbol{\nu}) \geq \text{ELBO}(\boldsymbol{\xi}, \boldsymbol{\nu}).$$

Maximizing ELBO with respect to  $\boldsymbol{\xi}$  gives a tighter bound on the log-marginal likelihood. Hence, a variational EM algorithm, similar as the one described in [24], can be used to efficiently optimize the variational parameters  $\boldsymbol{\xi}$  and the hyperparameters  $\boldsymbol{\nu}$ . At the E-step, the ELBO is maximized with respect to  $\boldsymbol{\xi}$ , giving in that way a better approximation to the log-marginal likelihood and then, at the M-step, the updated ELBO is maximized with respect to  $\boldsymbol{\nu}$ . Nevertheless, we found empirically that the optimization of ELBO converges faster to a local maximum when the M-step is ignored and no prior information is incorporated into our VI framework. We postulate this behavior stems from the large amount of data available in our experiments which provides enough information to train our model efficiently without any prior information needed. Hence, the only parameters we need to optimize are the variational parameters  $\boldsymbol{\xi}$  using the following objective function

$$\mathbb{E}_{q_{\boldsymbol{\xi}}} [\log p(\mathcal{D}|\boldsymbol{\theta}_f)] \approx \frac{1}{L} \sum_{l=1}^L \log p(\mathcal{D}|\boldsymbol{\theta}_f^{(l)}). \quad (17)$$

This objective function is the same as the ELBO in (11) without the regularization term  $\text{KL}[q_{\boldsymbol{\xi}}(\boldsymbol{\theta}_f) \parallel p_{\boldsymbol{\nu}}(\boldsymbol{\theta}_f)]$ , which can be obtained when the chosen prior  $p_{\boldsymbol{\nu}}(\boldsymbol{\theta}_f)$  is identical to the variational distribution  $q_{\boldsymbol{\xi}}(\boldsymbol{\theta}_f)$ . Since the choice of prior has negligible importance in the presence of large amount of data and empirical evidence showed that faster convergence is attained by ignoring the KL-term, we opted to optimize the only the variational parameters using (17).

## B Extra experimental details

The exact experimental setups for each of the methods used in Section 5.1 are discussed here.

All methods were trained for 2000 epochs using batches of size 32 and setting as default optimizer Adam [52]. We also used the log-likelihood of the validation dataset for early stopping a method that does not improve its log-likelihood for a hundred consecutive epochs. This was not necessary for the three VI-based methods since no sign of overfitting was observed. However, this was crucial for the NN-based SAHP where overfitting was common in all four datasets.

Regarding hyperparameter tuning, each method has its own set of hyperparameters that requires thorough tuning. The choice of each set of hyperparameters was based on the configuration that maximized the log-likelihood on the validation dataset by grid-searching over the parameter space. More accurately, for each method we have:

**VI-EXP.** For each dataset, we tried  $\text{decay} \in \{0.1, 0.5, 1, 2, 4, 8, 16, 32\}$ . We chose  $\text{decay}=2$  for MIMIC dataset,  $\text{decay}=0.1$  for SOF,  $\text{decay}=16$  for MOOC, and  $\text{decay}=0.1$  for Retweets.



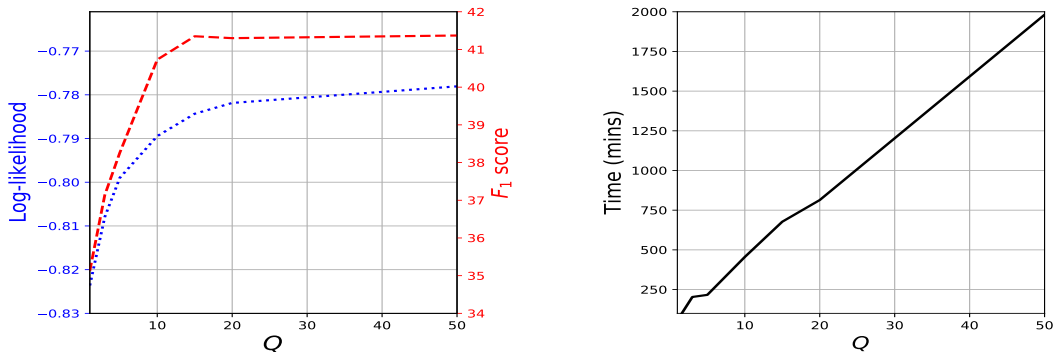


Figure 3: The values of log-likelihood (left panel, blue dotted line),  $F_1$  score (left panel, red dashed line), and training time (right panel, black solid line) as a function of the number of cut-off points  $Q$  for our model VI-DPP trained over the Retweet dataset. The log-likelihood computation here takes into account only the marks.

**VI-GAUSS.** Here we had to tune two hyperparameters, the number of Gaussian basis  $M$  and the cut-off time  $T_c$ . The center of the  $m$ -th Gaussian kernel is  $t_m = T_c \cdot (m - 1)/M$  and its scale is given by  $s = T_c/(\pi M)$ ; see [24] for more details. For each dataset, we tried  $M \in \{1, 2, 4, 10, 15, 20, 30\}$  and  $T_c \in \{M/4, M/2, M, 2M, 3M, 4M, 5M, 8M, 16M\}$ . We chose  $M = 2, T_c = 4$  for MIMIC dataset,  $M = 20, T_c = 60$  for SOF,  $M = 4, T_c = 64$  for MOOC, and  $M = 30, T_c = 150$  for Retweets.

**SAHP.** Hyperparameter tuning was the most challenging one for this model since it comes with a large number of hyperparameters due to its neural net dependence. For example, we have the number of hidden units, number of layers, number of attention heads and dropout ratio for neural net’s weights. We also found important setting a warm-up schedule to increase and then reduce learning rate throughout optimization as suggested in [16]. We found that four hidden layers, four attention heads, dropout=0.1, and initial learning rate equals to  $3 \times 10^{-5}$  worked well across all dataset and thus we kept that values fixed. We chose 32 hidden units for MIMIC dataset, 128 for both SOF and MOOC, and 64 for Retweets.

**VI-DPP.** For our method the only parameter needed tuning was the number of cut-off points  $Q$ . We chose  $Q = 1$  for all datasets except Retweets where  $Q = 15$  was used. Other parameters such as momentum term and number of MC samples  $L$  were set as in [24], i.e. 0.5 for momentum term and  $L = 1$ .

Regarding the learning rate for VI-EXP/GAUSS, it was set 0.05 and kept fixed over all datasets. Similarly, for VI-DPP a common a learning rate was used with value 0.03

## C Datasets

We provide a short description on the four real-world datasets used in Section 5.1.

**MIMIC-II (MIMIC).** The Multiparameter Intelligent Monitoring in intensive Care (MIMIC-II) is a medical dataset consisted of clinical visit records of intensive care unit patients for seven years. There are records of 650 patients/sequences where each one contains the time of the visit

and the diagnosis result of this visit. There are  $U = 75$  unique diagnosis results. The goal is to predict the time and the diagnosis result of a patient.

**Stack Overflow (SOF).** The data comes from the well-known question-answering website Stack Overflow<sup>2</sup> where users are encouraged to answer questions so they can earn badges. There are  $U = 22$  different types of badges. The data has been obtained is from 01/01/2012 to 01/01/2014. Each sequence corresponds to a user and each event gives the time and the type of badge a user has been awarded.

**MOOC.** This dataset consists of the interactions of students on a massive open online course (MOOC) on XuetangX<sup>3</sup>, one of the largest MOOC platforms in China. The interactions are  $U = 98$  in total, and some examples are video viewing, answer submission etc. A sequence contains the interactions with their corresponding occurrences of a given user.

**Retweets (RET).** The Retweets dataset includes retweets sequences, each commenced with an original tweet. Each retweet is described by the time it occurs and the type of this retweet; we have  $U = 3$  retweet types: small, medium and large ones, depending on the popularity (number of followers) of the retweeter. The aim is to predict when the next retweet will be and how popular the next retweeter will be.

## D Football association data

A concise description of the marks  $u$  used for our case study in Section 5.2 is provided in Table 3 while more details can be found in [17].

## E Links of videos

The links of the videos for each of the four matches of Figure 2 accompanied with the right time interval of the goal in the video in parentheses, the date of the match, the name of the MC's player who scored the first goal, and the final score.

**MC vs Newcastle United.** *Url:* [https://www.youtube.com/watch?v=ycnM\\_V273Zc&ab\\_channel=HDKoooralive](https://www.youtube.com/watch?v=ycnM_V273Zc&ab_channel=HDKoooralive) (see 0:00 - 1:00) *Date:* 19/08/2013 *Scorer's name of first goal:* Silva *Final score:* 4-0

**MC vs Manchester United.** *Url:* [https://www.youtube.com/watch?v=EcpGNaQDo7c&ab\\_channel=manchesterunitedforlife](https://www.youtube.com/watch?v=EcpGNaQDo7c&ab_channel=manchesterunitedforlife) (see 0:00 - 1:20) *Date:* 22/09/2013 *Scorer's name of first goal:* Aguero *Final score:* 4-1

**MC vs Swansea City.** *Url:* [https://www.youtube.com/watch?v=FEI7pasX5bY&ab\\_channel=WARLON58](https://www.youtube.com/watch?v=FEI7pasX5bY&ab_channel=WARLON58) (see 0:00 - 0:30) *Date:* 01/12/2013 *Scorer's name of first goal:* Negredo *Final score:* 3-0

---

<sup>2</sup><https://archive.org/details/stackexchange>

<sup>3</sup><http://moocdata.cn/challenges/kdd-cup-2015>

Table 3: Mark type description for the football association data. The value of  $p$  can be either “H” or “A” depending on whether an event is triggered by the home or away team, respectively. The events with the “H” prefix have  $u \in \{1, \dots, 15\}$  while “A” events have  $u \in \{16, \dots, 30\}$ . If  $u$  is a “H” event then  $u + 15$  is the corresponding “A” event, and thus, we have  $U = 30$  distinct event types.

$u$	Label Name	Description
1 or 16	p_Win	A player of the $p$ team regains possession of the ball from the opponent.
2 or 17	p_Dribble	A player of the $p$ team takes the ball forward with repeated slight touches.
3 or 18	p_Pass_S	A player of the $p$ team gains possession of the ball from a pass coming by one of his teammates.
4 or 19	p_Pass_U	A player of the $p$ team failed to pass successfully the ball to one of his teammates.
5 or 20	p_Shot	A player of the $p$ team shots the ball at opponent’s goal. Attempts where the ball misses the target are also included.
6 or 21	p_Keeper	The goal keeper of the $p$ team takes possession of the ball into their hands by picking it up or claiming a cross.
7 or 22	p_Save	The goal keeper of the $p$ team prevents a shot from crossing the goal line.
8 or 23	p_Clear	A player of the $p$ team moves the ball away from his goal area to safety.
9 or 24	p_Lose	A player of the $p$ team loses possession of the ball.
10 or 25	p_Goal	A player of the $p$ team scores a goal.
11 or 26	p_Foul	A player of the $p$ team executes a free-kick due to a previously occurred foul.
12 or 27	p_Out_Throw	A player of the $p$ team sends the ball out-of-play.
13 or 28	p_Out_GK	The goal keeper of the $p$ team sends the ball out of play.
14 or 29	p_Out_Corner	A player of the $p$ team sends the ball out of play over the $p$ team’s goal line.
15 or 30	p_Pass_O	A pass from a player of the $p$ team to one of his teammates who is judged guilty of the offside offence.

**Arsenal vs MC.** *Url:* [https://www.youtube.com/watch?v=PQQq1GVb0Lk&ab\\_channel=mrszippy](https://www.youtube.com/watch?v=PQQq1GVb0Lk&ab_channel=mrszippy) (see 0:00 - 0:57) *Date:* 29/03/2014 *Scorer’s name of first goal:* Silva *Final score:* 1-1

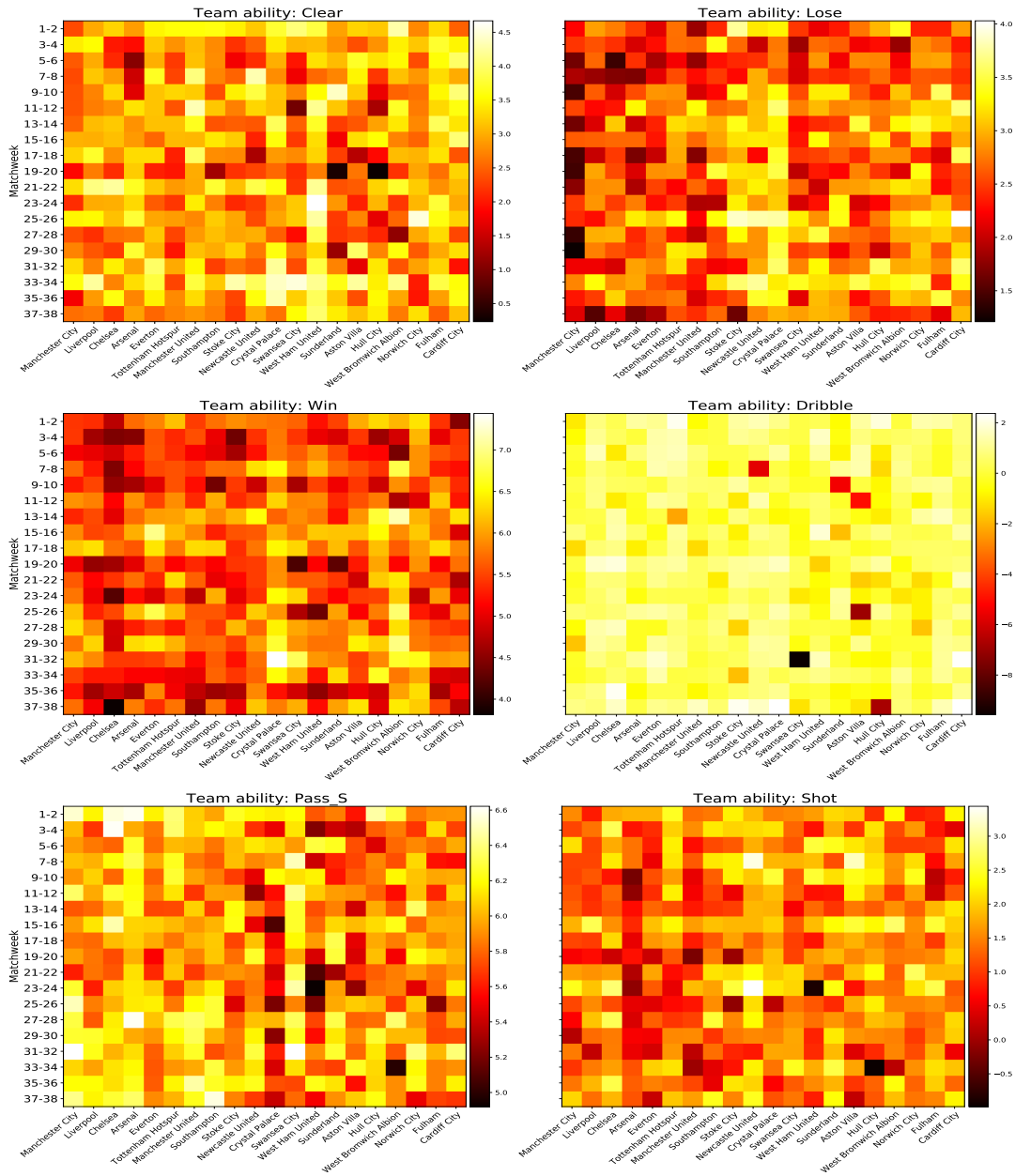


Figure 4: Heatmaps, as in Figure 1, illustrating the evolution of (i) (first row) the “Clear” ability, i.e. the ability of the team to move the ball away from the goal area (left panel), and “Lose” ability, i.e. the ability of the team to lose possession of the ball (right panel), (ii) (second row) the “Win” ability, i.e. the ability of the team to regain possession of the ball from the opponent (left panel), and “Dribble” ability, i.e. the ability of the team to take the ball forward with repeated slight touches (right panel), and (iii) (third row) the “Pass\_S” ability, i.e. the ability of the team to pass successfully (left panel), and “Shot” ability, i.e. the ability of the team to attempt shots at the opponents’ goal, including those missing the target (right panel)